

Article

Ore Genesis of the Dongping Gold Deposit in the Northern Margin of North China Craton: Constraints from In-Situ Major, Trace Elemental Analysis of Magnetite and Pyrite

Chengyang Wang ^{1,2,3,*}, Jiajia Yu ¹, Yunsheng Ren ^{2,3}, Junkang Zhao ⁴ and Zhenjun Sun ^{2,3}

¹ MNR Key Laboratory of Metallogeny and Mineral Assessment, Institute of Mineral Resources, Chinese Academy of Geological Sciences, Beijing 100037, China; yujia_2021@163.com

² School of Earth Sciences, Institute of Disaster Prevention, Sanhe 065201, China; rys@cidp.edu.cn (Y.R.); szj@cidp.edu.cn (Z.S.)

³ Hebei Key Laboratory of Earthquake Dynamics, Sanhe 065201, China

⁴ Institute of Geological Exploration, Zijin Mining Group Co., Ltd., Xiamen 361006, China; zhaojunkang@163.com

* Correspondence: wcy@cidp.edu.cn



Citation: Wang, C.; Yu, J.; Ren, Y.; Zhao, J.; Sun, Z. Ore Genesis of the Dongping Gold Deposit in the Northern Margin of North China Craton: Constraints from In-Situ Major, Trace Elemental Analysis of Magnetite and Pyrite. *Minerals* **2022**, *12*, 978. <https://doi.org/10.3390/min12080978>

Academic Editor: Maria Economou-Eliopoulos

Received: 14 June 2022

Accepted: 27 July 2022

Published: 31 July 2022

Publisher's Note: MDPI stays neutral with regard to jurisdictional claims in published maps and institutional affiliations.



Copyright: © 2022 by the authors. Licensee MDPI, Basel, Switzerland. This article is an open access article distributed under the terms and conditions of the Creative Commons Attribution (CC BY) license (<https://creativecommons.org/licenses/by/4.0/>).

Abstract: The Zhangxuan district in North China, also known as Northwestern Hebei “Golden Triangle,” develops many intrusion-hosted lode-gold deposits. The Dongping gold deposit in the Zhangxuan district is well known for its unique hosting of rocks and ore mineral assemblages. Magnetite and pyrite are common minerals that widely exist in ores of the Dongping deposit. To get a better understanding of the evolution of the ore-forming fluids responsible for mineralization, we report on an integrated study on the electron microprobe analysis (EMPA) and laser ablation-inductively coupled plasma-mass spectrometry (LA-ICP-MS) analysis of magnetite and pyrite from the deposit. The major results are as follows: The magnetite grains from the Dongping deposit show a variable content of major and trace elements such as Ti, Al, Si, Fe, Mn, Cr, Na, V, and Co, and the majority of the magnetite contain low Ti contents, revealing potential properties of hydrothermal magnetite. The flat time-resolved signals of LA-ICP-MS imply that the majority of trace elements in magnetite exist in the form of isomorphism, except for some incompatible trace elements. Magnetites from the Dongping deposit have compositional characteristics of hydrothermal origins, and the genetic discriminant diagrams of Ti–V, Ti–Ni/Cr or (Ca + Al + Mn)–(Ti + V) show that they may be originated from magma differentiated hydrothermal solutions. Co, Ni in pyrite from Dongping mainly enter the lattice via isomorphism, and Cu, Zn, Ag, W, Sn, Au, Pb, and Bi are partitioned into pyrite as micro/nano-mineral inclusions. The Co, Ni content, and the Ni/Co ratios, indicated that the temperature of the ore-forming fluids has decreased from Py-1 to Py-2, and the enrichment of Au in Py-2 may be related to the cooling and boiling of the fluids.

Keywords: EPMA; LA-ICP-MS; magnetite; pyrite; Dongping deposit; northern margin of North China Craton

1. Introduction

The intrusion-hosted lode gold deposits provide China with the largest gold reserves [1,2]. The North China Craton (NCC), which is one of the three famous Precambrian cratons globally, develop a large quantity of intrusion-hosted deposits along its margins [3–5]. The Zhang-Xuan area is located along the northern margin of North China Craton, and has always been regarded as one of the most famous gold mining districts in Northern China (Figure 1). Since the Dongping gold deposit in the 1980s, several ore deposits showing similar geological characteristics have been successively discovered, evaluated, and mined in this area. Based on their distinctive ore mineral assemblages and hosting wall rocks, Chinese geologists have proposed that the Dongping and other similar

deposits in the adjacent areas represent a particular type of gold mineralization, named the ‘Dongping-type’ deposit [6]. Among these deposits, the Dongping gold deposit is the largest deposit, with proven gold reserves of >100 tons in the Zhangxuan district. It is also the most representative deposit, which can be used as an example to explore its geological characteristics and formation mechanism [7].

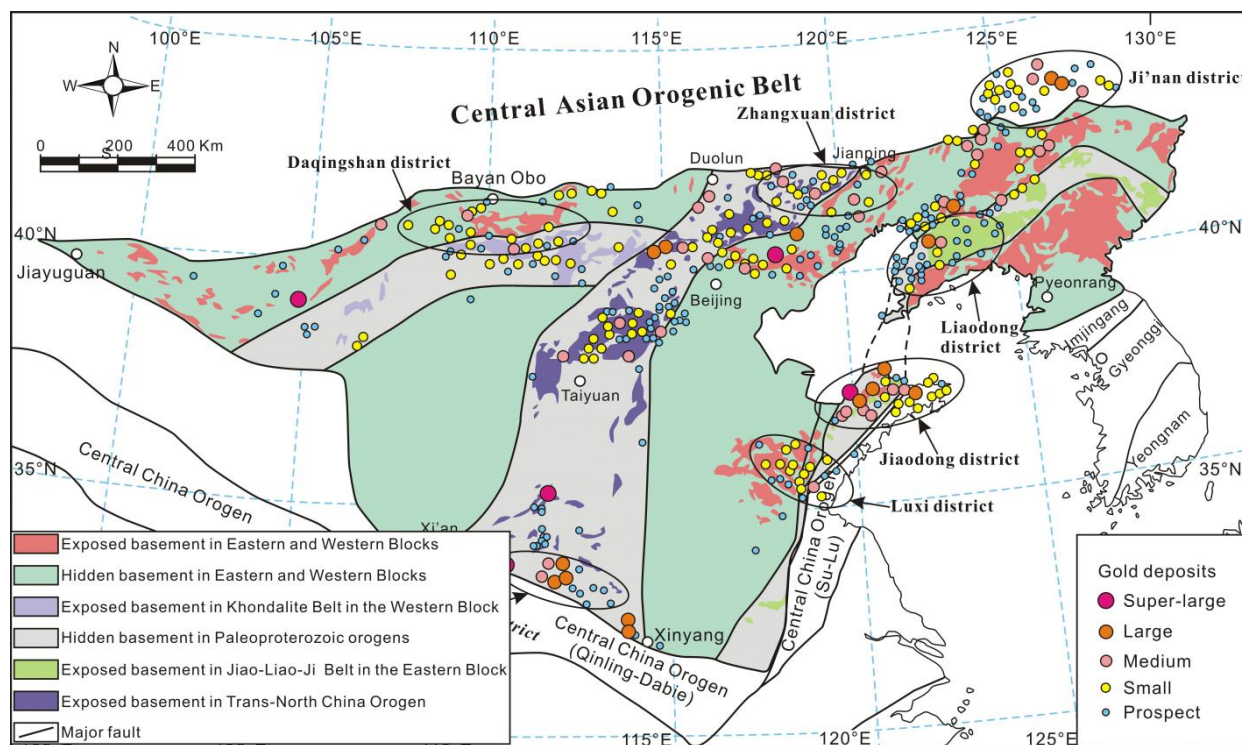


Figure 1. The distribution of gold deposits in the North China Craton (modified after Zhao et al. [12]; Deng and Wang [13]; He et al. [14]; Li and Santosh [15]).

During past decades, many studies concentrating on the genesis, fluid-rock interaction, ore-forming physicochemical conditions of the Dongping deposit have been conducted. A significant achievement obtained by previous research is that the Dongping deposit is derived from deep-derived alkaline magma [8–11]. High precise in situ chemical analysis can provide enhanced information on the metallogenic physicochemical conditions, and the nature of ore-forming fluids. Therefore, we present the first research on the in-situ element analysis for pyrite and magnetite from the deposit, through LA-ICP-MS and EPMA methods. The primary purpose of this research is to determine the genesis and evolution of the deposit.

2. Regional and Ore District Geology

Tectonically, the Zhangxuan district is located in the middle part of the northern margin of the North China Craton (Figure 2). As one of the most important gold-producing bases in China, the northern margin of the North China Craton hosts approximately 900 individual gold deposits [16]. In recent years, due to its excellent resource potential and associated Te mineralization, the gold deposits in Dongping and its adjacent areas (also known as Zhangxuan district) have attracted great attention from Chinese geologists and government officials.

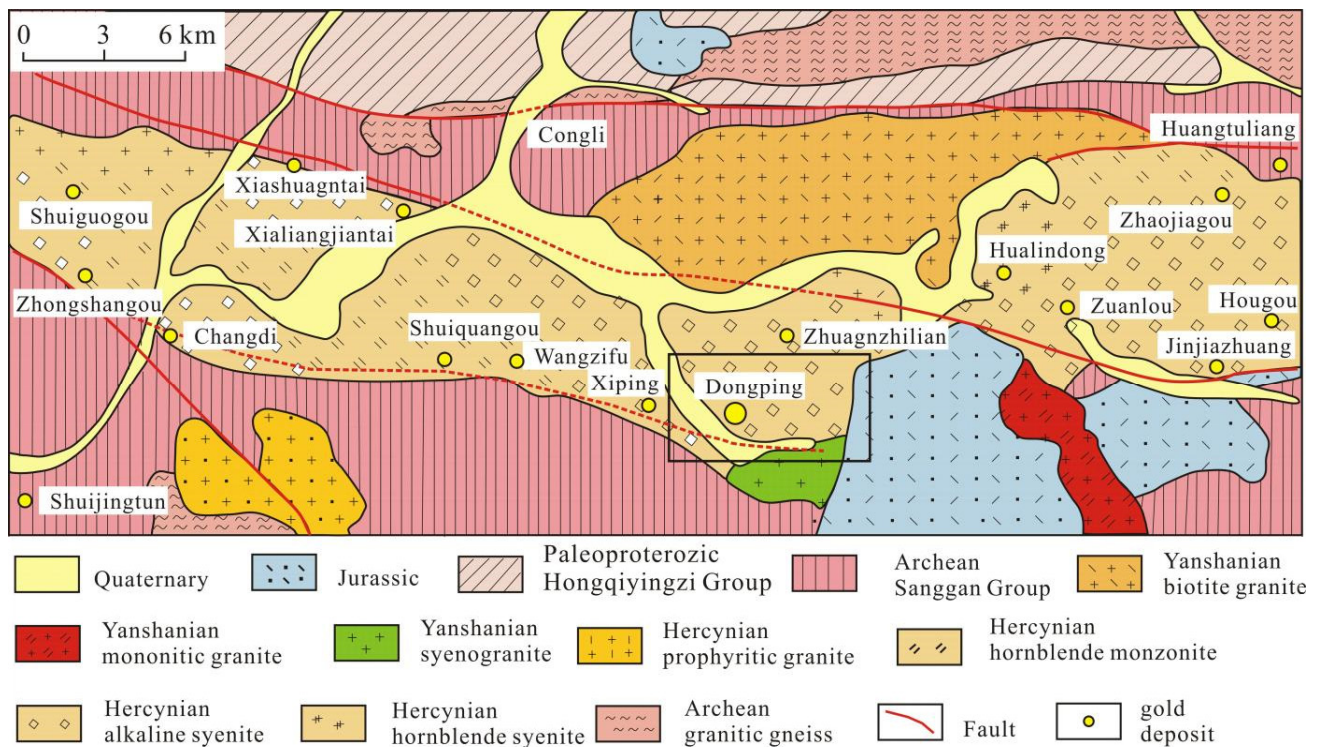


Figure 2. Geological sketch map of the area surrounding the Dongping gold deposit in the Hebei province (modified after Song and Zhao [17]; Li et al. [18]).

The outcropping successions in the regional area mainly consist of the Archean Sanggan Group and the Jurassic meta-sedimentary rocks. The Archean Sanggan Group represents the oldest crystalline basement in this area, and is composed of metamorphic rocks, including gneiss, plagioclase-amphibolite, and granulite. The Jurassic volcanic-sedimentary rocks, dominated by rhyolite, rhyodacite, trachyte, and pyroclastic flows, are widely distributed in this area. Three cycles of tectonic-magmatic activities have been recorded in the Dongping goldfield region: (1) the Archean-Proterozoic intrusive diorites, peridotites, and pyroxenites; (2) the Devonian alkaline intrusive rocks, mainly including the Shuiquangou igneous complex; (3) the Mesozoic alkali granite plutons, which intruded the Archean basement and the margins of the Shuiquangou complex. Gold deposits in the regional area are mainly located within the Shuiquangou complex [19,20]. The Mesozoic plutons (formed at ca. 140 Ma) are exposed in the margins of the Shuiquangou complex, and they are likely to be related to underplate of the crust. The east-west trending Shangyi–Chongli–Chicheng fault is the most remarkable tectonic feature in the regional area, and the Shuiquangou alkaline intrusive complex was emplaced after the latest shearing along with the Shangyi–Chongli–Chicheng fault system [20]. The NE-trending Zhongshangou–Honghuabei–Shangshuiquan fault might be the main conduit for the gold-bearing hydrothermal activities. Orebodies from this area are hosted in third-order NNE- and NW- trending fractures [17].

The representative gold deposits in the Zhangxuan district are mainly composed of Dongping, Zhongshangou, Shuijingtun, Xiaoyingpan, Hougou, Huangtuliang, Guzuizi, Zhangquanzhuang, Beigangou, Dayingz, and Shiziling (Figure 2). Based on the location and occurrence of the orebodies, the above deposits can be divided into two major types, namely the Dongping type and the Xiaoyingpan type. The Dongping type deposits are distributed within the Devonian Shuiquangou alkaline complex, while the Xiaoyingpan deposits are mainly hosted in the Archean high-grade metamorphic rocks of the Sanggan Group [8]. Although numerous isotopic dating results have been published, the ages of gold mineralization in this area are still controversial.

3. Ore Deposit Geology and Mineralization Characteristics

The Dongping deposit is located in Chongli County, Northwest Hebei Province, China. The latitude and longitude of the mining area are 40°50'47"~40°53'34" N and 115°18'17"~115°24'08" W, respectively.

Mineralization of the deposit occurs at the contact zone between the Devonian Shuiquangou complex and the Late Archean rocks. In addition to the above two geologic units, major geological units exposed in this area include those of the Early Proterozoic Hongqiyngzi Group, Middle Proterozoic Changcheng Group, and Jurassic and Quaternary rocks. More than 70 gold veins or swarms have been discovered in the mining area, and only five of them have attained economic concentrations and been mined. Veins of the deposit are mainly hosted by Devonian intrusions and are controlled by a group of NE- and NW-trending faults (Figure 3). The lengths of ore veins ranged from several hundred to more than one thousand meters. Ores in the study area are characterized by rich telluride but low sulfide contents [17]. The identified telluride minerals mainly include calaverite, petzite, altaite, hessite, krennerite, and stutzite [9]. Quartz vein and altered syenite type ores are developed in the deposit; the Te and Au contents are quite different between the two kinds of ores. Generally, the widespread and intensive hydrothermal alteration changed the composition, structure, and texture of the wall rock, and finally formed the vein-like orebodies. In this case, the boundary between orebody and its wall rock is not well defined. In the other case, silica-rich ore-bearing hydrothermal fluids filled in along the fracture and finally formed the auriferous quartz veins, which have a distinct boundary with the wall rocks. Based on the mineral assemblages and their crosscutting relationships, previous scholars have divided the mineralization and alteration of the deposit into four main stages: (I) early silica-potassium alteration stage, (II) magnetite-hematite-pyrite-quartz stage, (III) Au bearing polymetallic sulfide-telluride quartz stage, and (IV) carbonate-quartz stage (Figures 4 and 5; [21]).

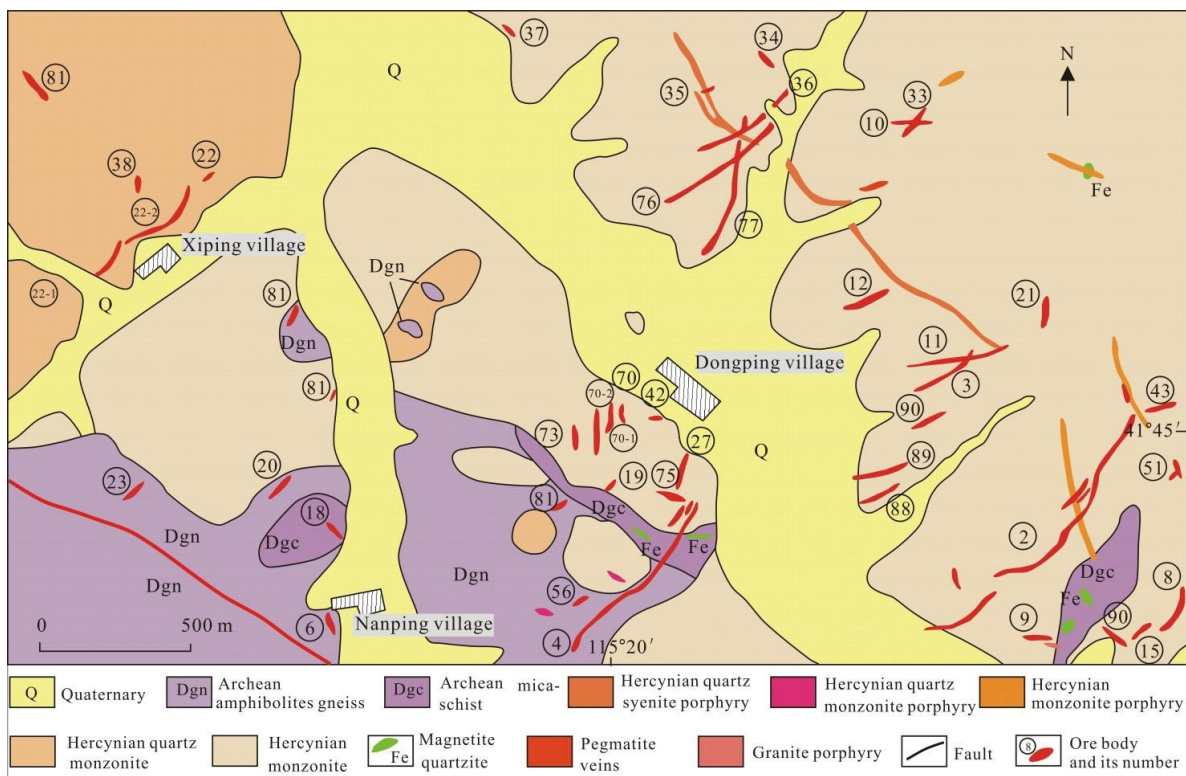


Figure 3. Simplified geological map of the Dongping gold deposit (modified after Wang et al. [8]).

Stage Minerals	stage I	stage II	stage III	stage IV
K-feldspar	██████████			
Quartz	██████████	██████████	██████████	██████████
Garnet	-----	-----	-----	
Epidote		██████████	██████████	
Sericite		-----		
Calcite				██████████
Specularite	██████████			
Pyrite	-----	-----		
Magnetite		██████████		
Native gold		-----		
Chalcopyrite		-----		
Galena		██████████		
Pyrrhotite			
Telluride		-----		

Figure 4. Paragenetic sequence for the Dongping deposit.

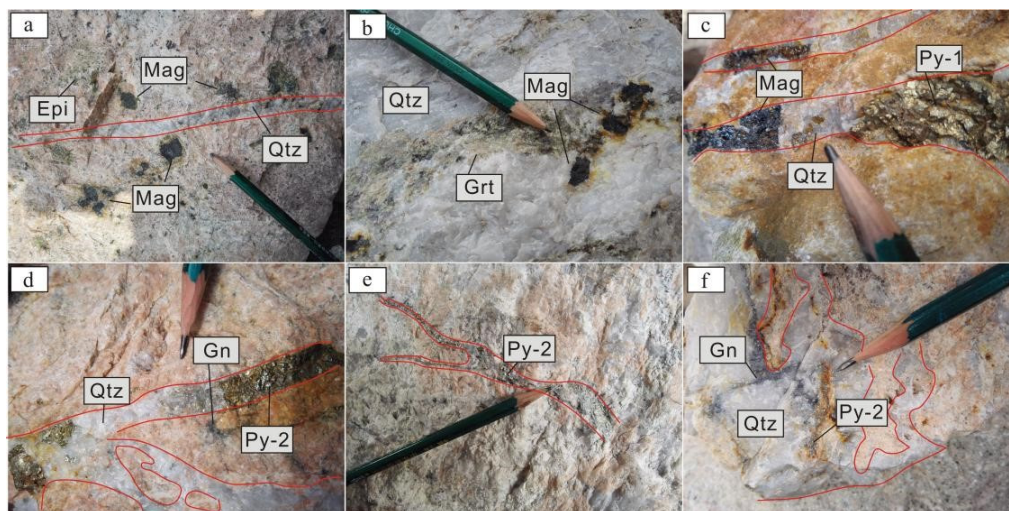


Figure 5. Representative photos of hand-specimens from the Dongping deposit: (a) Potassic rocks containing euhedral magnetite are crosscut by quartz vein; (b) Epidote, garnet, and magnetite coexist in quartz vein; (c) Garnet-magnetite-pyrite-quartz vein crosscut potassic rock; (d) Polymetallic sulfide quartz vein containing pyrite; (e) Quartz vein containing fine-grained pyrite aggregates; (f) Irregular quartz vein containing galena and pyrite. Epi—epidote; Gn—galena; Grt—garnet; Mgt—magnetite; Py—pyrite, Qtz—quartz.

4. Samples and Analytical Methods

4.1. Sample Descriptions

The iron oxide minerals within ores from the Dongping deposit are always neglected by previous studies. The magnetites from Dongping deposit have two occurrences: Mgt-1 developed in potassic igneous rocks, this type of magnetite exhibits irregular and anhedral

shapes. Mgt-2 refers to magnetite occurred in the quartz veins. Compared with Mag-1, Mag-2 is favorable to form in the edge of quartz vein. Magnetite in this deposit always coexist with hematite, and show homogeneous internal textures in reflected light images. Pyrite is widespread in Dongping ores. Two pyrite types were identified within the ores, and denoted as Py-1 and Py-2. Py-1 is dominantly characterized by coarse euhedral crystals. In some cases, Py-1 coexists with magnetites in quartz veins (Figure 5). Previous studies suggest that no significant gold mineralization was associated with Py-1. Py-2 refers to the pyrite in tellurides- sulfide-quartz veins. This type of pyrite generally occurs as fine-grain aggregates in quartz veins and is replaced by other sulfide minerals. The associated sulfide minerals of Py-2 include chalcopyrite, galena, sphalerite, molybdenite, etc. (Figure 6).

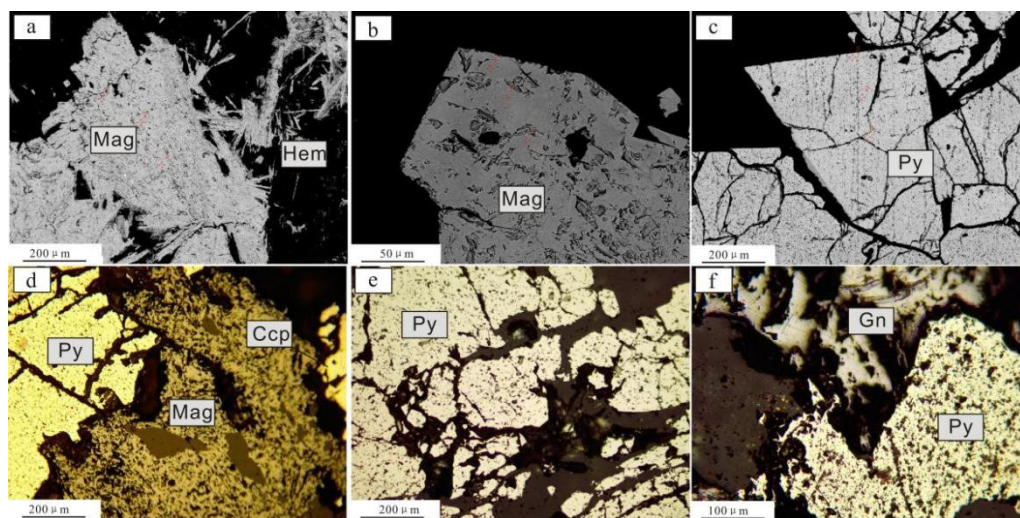


Figure 6. Photomicrographs showing textures and occurrences of magnetite/pyrite in the Dongping gold deposit: (a) BSE image of magnetite and hematite; (b) BSE image of euhedral magnetite; (c) BSE image of euhedral pyrite; (d) Reflected light image of magnetite-pyrite-chalcopyrite; (e) Reflected light image of pyrite aggregate; (f) Reflected light image of pyrite and galena. Ccp—chalcopyrite; Gn—galena; Py—pyrite; Mgt—magnetite; Hem—hematite.

4.2. Analytical Methods

Magnetite and pyrite samples of this study were mainly collected from Drilling Hole CK2, ZK1393, ZK1393, ZK301A, CK256, and open pit from the Dongping deposit. Based on the petrographic observations, 14 samples containing magnetite and pyrite were prepared for in-situ analysis. The EMPA analysis was conducted at the Wuhan Sample Solution Analytical Technology Co., Ltd., Wuhan, China. An EOL JXA-8230 electron probe micro-analyzer was used in this analysis. The accelerating voltage, current, and beam size of the EMPA are 20 kV, 5 nA and 1 μm , respectively. Peak and background counting times for Ni, Co (in pyrite), and Ca, Si (in magnetite) were 20 and 10 s, respectively. Pure FeS_2 , Sb_2Te_3 , ZnS , Sb_2Te_3 , $(\text{Fe, Ni})_9\text{S}_8$, Co, FeAsS , PbS , CuFeS_2 , Bi_2Se_3 , Au, and Ag were used as the standard materials for pyrite. Crystal analyzer used in this analysis included LIFH, PETH, PETJ, LIF, TAP. The test elements and their detection limits (mass fraction) are as 243×10^{-6} , Se 103×10^{-6} , Fe 138×10^{-6} , Co 125×10^{-6} , Ni 128×10^{-6} , Cu 161×10^{-6} , Zn 190×10^{-6} , Au 207×10^{-6} , S 42×10^{-6} , Pb 240×10^{-6} , Ag 85×10^{-6} , Te 94×10^{-6} , V 118×10^{-6} , Ti 91×10^{-6} . TiO_2 , $\text{CaMnSi}_2\text{O}_6$, $\text{NaAlSi}_2\text{O}_6$, $(\text{Mg, Fe})_2\text{SiO}_4$, $\text{Mg}_3\text{Al}_2\text{Si}_3\text{O}_{12}$, SiO_2 , $(\text{Fe, Ni})_9\text{S}_8$, Mn, FeCr_2O_4 , V, KAlSi_3O_8 , Co was used as the standard materials for magnetite. As the trace element contents of magnetite were mostly below the detection limits, EMPA results for some elements were not present in this article.

LA-ICP-MS analysis can provide enhanced resolution for trace element contents, we therefore further conducted in situ trace element research through the LA-ICP-MS method at the same laboratory as the EMPA analysis. The analysis was performed using a COMP-exPro Laser Ablation system coupled with an Agilent 7700e ICP-MS. The wavelength and

maximum energy of the excimer laser were 193 nm and 200 mJ, respectively. Helium and argon were applied as the carrier and make-up gas, respectively. The spot size used during the analyses were 26 μm . Each spot analysis includes a ~ 20 s background acquisition and a ~ 60 s data acquisition. Visible mineral inclusions and possible contamination were avoided during the examination. Trace element compositions of pyrite were calibrated by reference materials NIST 610 and NIST 612, and the reference materials used for magnetite composition calibrating were NIST 610, BHVO-2G, BIR-1G, and BCR-2G. Detailed analytical procedures are available by Hu et al. [22]. Data reduction and offline data processing were performed by ICP MS DataCal and Iolite software [23].

5. Analytical Results

5.1. Magnetite

Element analysis of magnetite by EMPA included K_2O , CaO , TiO , Al_2O_3 , SiO_2 , FeO , MnO , Cr_2O_3 , Na_2O , MgO , V_2O_3 , CoO , and NiO (Table 1). The analytical results of EMPA reveal that the two types of magnetite from Dongping have similar element compositions. The Al_2O_3 , Na_2O , MgO , and NiO contents of magnetite are mostly below or marginally higher than the detection limit. The maximum TiO_2 content determined by EMPA is 0.039 wt.%, revealing a characteristic of low Ti magnetite. The FeO , MnO , Cr_2O_3 , and CoO contents range 88.538–92.695 wt.%, 0.080–0.195 wt.%, 0.008–0.132 wt.%, and 0.100–0.197 wt.%, respectively. The average V_2O_5 contents of Mag-1 and Mag-2 are 0.003 wt.% and 0.099 wt.%, respectively. Comparatively, the Mag-2 has higher V_2O_5 contents than Mag-1.

Table 1. Selected EPMA analyses of magnetite grains from the Dongping deposit (wt.%).

No.	Al_2O_3	SiO_2	FeO	MnO	Cr_2O_3	V_2O_3	Total
MT-1	0.003	0.007	91.78	0.24	0.115	-	92.28
MT-2	0.012	0.021	91.63	0.162	0.132	-	92.10
MT-3	-	-	91.82	0.164	0.096	0.012	92.24
MT-4	0.013	0.041	92.05	0.107	0.127	-	92.51
MT-5	0.016	-	91.866	0.102	0.088	0.007	92.25
MT-6	0.012	0.073	91.77	0.119	0.119	-	92.23
MT-7	-	0.01	92.69	0.08	0.048	0.257	93.28
MT-8	-	-	91.55	0.08	0.101	0.281	92.20
MT-9	-	0.012	91.71	0.059	0.046	0.278	92.34
MT-10	0.183	0.785	90.50	0.039	0.038	0.022	91.77
MT-11	0.027	0.346	90.79	0.025	0.008	-	91.34
MT-12	-	-	91.95	0.037	0.033	0.022	92.19
MT-13	-	0.399	90.98	0.259	0.103	0.028	91.93
MT-14	0.141	0.765	89.77	0.248	0.025	0.065	91.30
MT-15	-	0.257	90.92	0.16	0.128	0.024	91.60
MT-16	0.24	1.281	89.88	0.099	0.046	0.071	92.19
MT-17	0.302	1.676	88.54	0.182	0.008	0.068	91.35
MT-18	0.284	1.98	88.60	0.195	0.023	0.082	91.78

Notes: “-” means the content of the element is below detection limit.

The analytical results of magnetite by LA-ICP-MS can be recognized as follows (Table 2): Magnetite from the Dongping deposit has around 1300–5100 ppm Si, 100–1200 ppm Al, and 100–5000 ppm Ca, and 50–150 ppm Mg. Mag-1 has V contents of 8.62–234 ppm, Co contents of 40.8–91.4 ppm, and Ni contents of 1.48–17.5 ppm, coupled with lower Cr (with an average of 35.6 ppm), Zn (with an average of 162 ppm), Ag (<0.028 ppm), W contents of (mostly <0.4 ppm) contents. Mag-2 has average V contents of 57.6 ppm, average Cr contents of 81.23 ppm, Co contents of 10.9–66.6 ppm, Ni contents of 0.52–4.49 ppm, Cu contents of 11.5–46.7 ppm, Zn contents of 258–1787 ppm, Ag contents of 0.037–4.23 ppm, W contents of 0.091–68.2 ppm, Pb contents of 41.59–1163 ppm. The Spot 7, Spot 8, and Spot 11 have extremely higher Ca contents (6.75 wt.% for Spot 7, 2.20 wt.% for Spot 8, and 2.69 wt.% for Spot 11, respectively). Spot 7 also has a higher Mn content, suggesting that invisible carbonate mineral inclusions probably exist in magnetite.

Table 2. Selected LA-ICP-MS analyses of magnetite grains from the Dongping deposit.

Sample No.	Al ₂ O ₃ wt. %	CaO wt. %	TiO ₂ wt. %	V ppm	Cr ppm	MnO wt. %	Fe wt. %	Co ppm	Ni ppm	Cu ppm	Zn ppm	W ppm	Pb ppm
DP-1-1	0.017	0.017	0.0011	12.9	127	0.18	71.78	83.0	8.35	-	104	0.40	7.90
DP-1-2	0.130	0.039	0.0049	183	11.0	0.10	71.36	83.8	7.93	1.42	66.9	60.1	24.34
DP-1-3	0.013	-	-	8.62	4.91	0.30	71.80	91.4	1.48	-	124	0.35	3.211
DP-1-4	0.043	0.0064	0.0050	59.3	21.6	0.094	71.95	40.8	17.5	110	209	0.043	194.12
DP-1-5	0.058	0.022	0.0065	173	33.1	0.095	71.50	41.7	6.67	150	276	0.16	281.76
DP-1-6	0.074	0.045	0.0092	234	40.3	0.19	71.41	42.3	15.4	69.7	196	0.085	128.49
DP-2-7	0.220	9.26	0.0019	69.2	629	0.47	64.32	10.9	3.81	42.4	258	68.2	634.52
DP-2-8	0.140	3.03	0.0018	83.5	12.9	0.10	69.11	12.5	4.31	40.1	1707	40.0	1163.33
DP-2-9	0.048	0.029	0.0008	28.0	9.35	0.032	71.77	66.6	2.31	16.5	482	0.091	41.59
DP-2-10	0.024	0.020	0.0016	44.3	6.27	0.038	71.71	20.3	4.49	11.6	217	0.72	116.57
DP-2-11	0.31	3.69	0.0014	67.4	37.4	0.32	68.25	14.1	0.52	43.5	349	18.5	641.05
DP-2-12	0.15	0.067	0.0020	75.6	40.6	0.086	71.23	26.5	3.51	120	580	4.18	585.00
DP-2-13	0.040	0.029	0.0008	21.9	13.5	0.079	71.70	28.8	3.37	15.2	374	0.24	130.87
DP-2-14	0.53	0.053	0.0009	77.6	18.9	0.18	70.16	34.3	3.69	46.7	1188	0.15	359.56
DP-2-15	0.038	0.023	0.0006	9.44	32.0	0.088	74.89	31.6	2.78	11.5	374	1.50	247.77
DP-2-16	0.20	0.036	0.0053	99.2	12.2	0.070	71.17	20.1	2.35	34.3	990	47.8	648.30

Notes: “-” means the content of the element is below detection limit.

5.2. Pyrite

Results of EMPA for pyrite from the Dongping deposit are given in Table 3. The major and minor element analysis of pyrite by EMPA mainly included Zn, Cu, Te, Sb, Se, Co, Ni, As, Au, Pb, and Ag. The average Fe, S, and Co contents are 46.05 wt.%, 53.80 wt.%, and 0.084 wt.% for Py-1; 46.10 wt.%, 53.75.05 wt.%, and 0.076 wt.% for Py-2; The contents of Ag and other trace elements (Cu, Ni, Pb, Te, Sb, Se) in pyrite were close to or below the detection limits of EMPA. Compared with Py-1, Py-2 has higher Au and Pb contents (average at 0.012 wt.%), but lower Zn and Co contents.

Table 3. Selected EPMA analyses of pyrite grains from the Dongping deposit (wt.%).

Sample No.	Zn	Cu	Te	Se	Fe	Ni	Au	S	Pb	Total
DS-1-PY-1	-	0.008	0.01	0.029	45.76	0.001	0.019	53.466	0.004	99.38
DS-1-PY-2	-	-	-	-	45.99	0.013	0.004	53.547	0.016	99.67
DS-1-PY-3	-	0.014	-	-	46.03	-	0.012	53.701	-	99.84
ZS-1-PY-1	0.015	-	0.003	-	46.06	-	-	53.996	0.005	100.17
ZS-1-PY-2	0.014	0.018	-	-	46.19	0.001	0.033	54.075	0.015	100.43
ZS-1-PY-3	0.014	-	0.027	0.032	46.26	-	0.005	54.071	0.015	100.52
ZH-2-PY-1	0.009	0.006	-	-	45.76	-	-	53.724	-	99.82
ZH-2-PY-2	0.047	-	-	-	46.26	-	-	53.827	-	100.22
ZH-2-PY-3	0.005	0.005	-	0.009	46.24	0.001	0.039	53.12	0.035	99.56
DS-2-PY-1	0.008	-	0.013	-	46.21	-	-	53.911	-	100.23
DS-2-PY-2	-	-	-	-	46.08	-	-	54.025	-	100.207
DS-2-PY-3	0.002	0.006	0.002	0.003	46.05	-	-	53.919	-	100.08

Notes: “-” means the content of the element is below detection limit.

A total of 18 pyrite LA-ICP-MS analyses were completed on the Dongping gold ores, and the representative trace elements are selected to list in Table 4. The contents of Ti, Co, Ni, Cu, Zn, Ge, and Pb are all above detection limit values in all pyrite grains, and Mg, Al, V, Mo, Ag, W, Au, Tl, and Bi are below the detection limit in some pyrite grains. Py-1 records relatively higher abundances of Co (with an average of 16.9 ppm), and Ni (average at 10.4 ppm), while Py-2 show higher contents of Ti (1.73~1637 ppm), V (0~13 ppm) and Cr (0.42~3.47 ppm). Both Py-1 and Py-2 show wide ranges of P, K, Ca, Ti, Au, and Pb contents, etc. The As, W, Mo, Sn contents determined by LA-ICP-MS are primarily below the detection limits. The relatively lower contents detected by LA-ICP-MS are consistent with the EMPA results. Nevertheless, Spot 7, 8 and 9 of Py-2 have relatively higher abundances of Cu (0.77~3.42 ppm), Zn (0.77~1.60 ppm), W (0.55~41.8 ppm), Au (0.25~0.84 ppm), Pb (4.4~11.5 ppm), Bi (0.31~2.27 ppm), implying possible mineral inclusions.

Table 4. Selected LA-ICP-MS analyses of pyrite grains from the Dongping deposit.

Sample No.	Ti ppm	V ppm	Cr ppm	Mn ppm	Co ppm	Ni ppm	Cu ppm	Zn ppm	As ppm	Ag ppm	W ppm	Au ppm	Pb ppm	Bi ppm
PY-2-1	2.12	0.022	0.83	0.25	1.50	0.38	0.26	0.44	-	0.023	-	0.13	0.41	-
PY-2-2	2.11	0.014	0.98	0.096	3.67	1.24	0.25	0.62	0.83	0.0073	-	-	0.12	-
PY-2-3	1.73	-	0.68	-	1.09	0.89	0.17	0.66	0.073	-	0.0092	0.0001	0.36	-
PY-1-4	0.91	0.017	0.37	0.048	0.22	0.11	1.77	0.32	0.59	0.13	0.0092	0.19	3.43	1.25
PY-1-5	1.35	-	0.28	-	0.17	0.50	0.78	0.46	0.079	0.020	-	0.032	0.91	0.10
PY-1-6	1.42	-	0.31	0.068	1.25	1.10	0.13	0.53	-	0.0060	0.0037	-	0.029	0.0034
PY-2-7	1637	13.0	3.47	0.17	2.34	6.91	3.42	1.60	0.91	0.91	41.8	0.84	11.5	2.27
PY-2-8	225	5.48	0.84	-	1.68	2.15	1.88	0.47	0.43	0.82	24.2	0.38	4.18	0.32
PY-2-9	13.6	0.15	0.42	0.11	0.99	1.76	0.77	0.77	0.054	0.094	0.55	0.25	4.40	0.31
PY-1-10	1.36	0.0048	-	-	22.43	2.43	0.76	0.78	-	0.57	-	0.13	0.52	0.0005
PY-1-11	2.19	-	0.33	0.11	74.33	84.03	0.93	0.67	-	0.11	0.0086	-	0.039	0.0012
PY-1-12	1.21	0.014	0.61	-	51.15	12.24	0.41	0.34	0.30	-	-	0.011	0.21	0.0019
PY-1-13	1.66	-	-	-	4.01	1.94	0.56	0.54	0.055	0.033	-	-	0.38	-
PY-1-14	0.87	0.019	0.20	0.064	6.41	5.77	0.61	0.49	0.18	2.17	0.0054	0.61	0.48	0.0007
PY-1-15	2.04	0.0076	1.47	0.17	18.84	10.54	0.41	0.82	-	0.13	-	0.026	0.33	-
PY-1-16	2.04	0.0012	-	-	2.77	0.93	0.25	0.55	0.0043	0.66	-	0.0094	0.63	-
PY-1-17	0.88	0.026	1.18	-	2.68	1.10	5.18	0.58	0.40	25.01	-	6.43	5.17	0.018
PY-1-18	1.98	0.0000	0.46	0.18	19.08	4.90	1.75	0.73	0.027	5.07	0.0000	1.09	0.74	0.0063

Notes: “-” means the content of the element is below detection limit.

6. Discussion

6.1. Occurrences of Elements in Magnetite and Pyrite

Minor/trace elements in magnetite and pyrite can occur in different forms: (1) invisible solid solution within the crystal lattice, (2) invisible nanoparticles of minerals, and (3) visible micron-sized mineral inclusions [24–27]. As one of the most common spinel group minerals, magnetite is generally described by a formula of AB_2O_4 . Elements of Ti, V, Mn, Ni, Mg, Co, Zn, Al, Cr, or Ga can substitute into the magnetite crystal lattice via isomorphism, and these elements are thought to be compatible and detectable in magnetite [25,28]. While the incompatible elements (Al, Mg, Ca, K, and Na) probably enter magnetite structure as sub-micro-scale silicate inclusions [29]. Similar to magnetite, minor/trace elements in pyrite can substitute the Fe and S within the crystal lattice, or exist as nanoparticles and mineral inclusions of sulfides, silicates, and oxides [27]. Siderophile and chalcophile elements, including Co and Ni, are commonly entered via the lattice isomorphous replacement of Fe, while As can entered the lattice via isomorphous replacement of S. The element of Au, Ag, Cu, Pb, Zn, Te, Cr, V, Mn, Ga, Mo, Sn, and Sb generally exist as particles or nanoparticles in pyrite [30]. Mineral inclusions would significantly change the element contents detected by LA-ICP-MS, and may even result in some outliers. The following symbols can be used to identify the forms of elements in the LA-ICP-MS time-resolved depth profile: a flat time-resolved depth profiles indicate a pure mineral or the elements are incorporated into the internal structure of the mineral, while the peaks in time-resolved depth profiles are usually due to the mineral inclusions [31].

Our analyses shows that the majority of minor and trace elements in magnetite show flat patterns in the LA-ICP-MS time-resolved signal spectra; it is suggested that these elements have entered the magnetite lattice (Figure 7). Spot 7, 8, and 11 of our magnetite sample have relatively high Ca or Mn contents, indicating silicate minerals' inclusion in magnetite. Compared with magnetite, the LA-ICP-MS time-resolved signals of pyrite are more complicated. As shown in Figure 7, the signal intensities of Co and Ni are relatively stable and show similar distribution characteristics with that of Fe, inferring that Co and Ni enter pyrite as the form of isomorphism. However, the LA-ICP-MS time-resolved signals of Au, Ag, Cu, Pb, Te, and Bi are characterized by several apparent peaks. It is speculated that these elements may occur as invisible nanoparticles of sulfide, such as galena or tellurium-rich minerals.

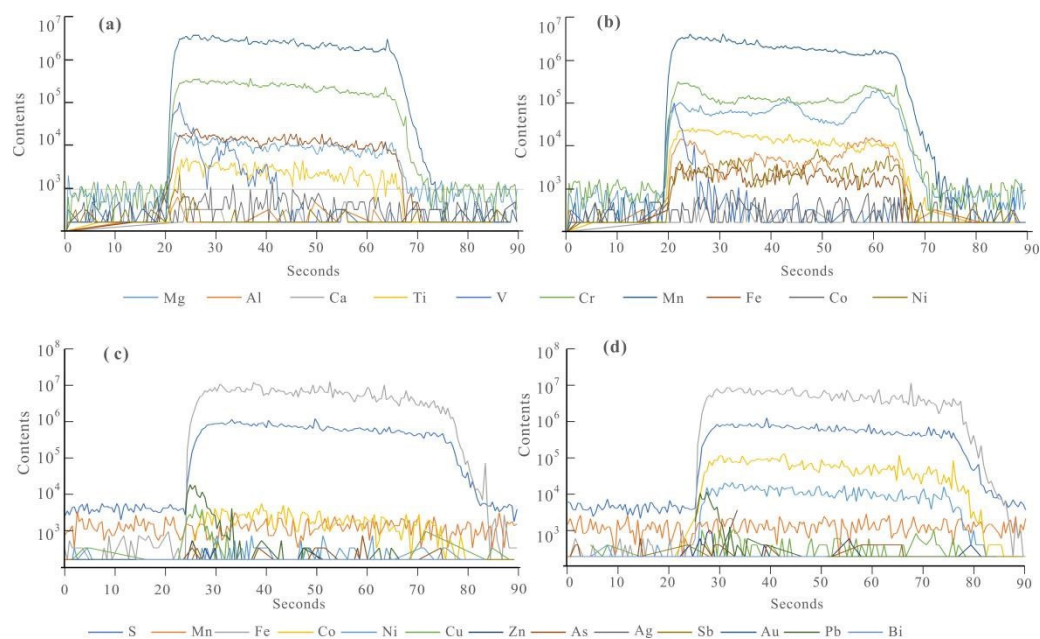


Figure 7. Representative time-resolved analytical signals of LA-ICP-MS analyses. (a,b) Magnetite; (c,d) Pyrite.

Pyrite is considered the primary mineral host for gold in the Dongping district. However, the Au contents in pyrite from both of the EMPA and LA-ICP-MS analysis are quite low, and the Au contents of some analyzed samples are even lower than the detection limit. The measured Au contents through EMPA (between 0 and 0.039 wt.%) in this study are higher than those through LA-ICP-MS (only reaching a maximum of 6.43 ppm). This phenomenon is also found in other intrusion-posted gold deposits; an explanation is that EPMA gives the detection limit for Au, which is much higher than this one of LA-ICP-MS.

6.2. Implications for the Mineral Genesis

6.2.1. Magnetite

Magnetite is commonly developed in magmatic, hydrothermal, sedimentary, and metamorphic environments [32], and it is also widely spread in skarn, IOCG and oxidized porphyry type mineralization systems. Nevertheless, the magnetite within ores is rare in intrusion-related gold deposits. Geochemical and geological factors, including temperature, oxygen fugacity, sulfur fugacity, the composition of the fluids, and fluid-rock reaction, can influence the element compositions in magnetite [24,25]. Temperature is one of the most important factors governing compositional variations in magnetite, and the Ti, V, Mn, Al, and Ga contents in magnetite are all sensitive to temperature [25]. Elements of Cr and V occur in various valence states, and their behavior is linked to the oxygen fugacity of the hydrothermal system. For example, V can appear as V^{3+} , V^{4+} , or V^{5+} ions in magmatic or hydrothermal solutions, while only V^{3+} can readily enter the magnetite crystal lattice. The increasing oxygen fugacity would convert V^{3+} to V^{4+} or V^{5+} , resulting in the decrease of V content in magnetite [25]. W mainly replaces the trivalent ions (e.g., Al^{3+} and Fe^{3+}), and the W content in magnetite is governed by both temperature and oxygen fugacity [33,34]. The Mg, Si, Al, and Mn contents in magnetite are remarkably influenced by the degrees of fluid-rock interaction in a skarn-type metallogenic system [35]. Based on the above conclusions, a range of elemental diagrams for distinguishing the magnetite genesis have been proposed, which provides us with good baselines for the source identification of magnetite from various ore types [32].

Two alternative mechanisms can explain the magnetite genesis of Dongping ores: (1) Previous research has found that Devonian Shuiquangou syenitic complex constitutes the most important hosting rocks for ores in this area, and the magnetite commonly occur

as an accessory mineral in Shuiquangou Complex [7]. Therefore, the magnetite from ores may capture, or inherit, from hosting igneous rocks. In this case, the magnetite should be formed at a higher temperature and show characteristics of magmatic origins. (2) Similar to porphyry or skarn system, magnetite of ores can form during a hydrothermal stage, and show geochemical features of hydrothermal magnetite. The magnetite compositions can discriminate the genetic type of magnetite. Mn, Ti, Cr, and Co are regarded as the most useful discriminator elements to differentiate magnetite type. Compared with hydrothermal magnetite, the igneous magnetite has, on average, higher Cr, Ti, V contents but lower Co contents [33].

In magnetite from the Dongping deposit, the Ni contents measured by LA-ICP-MS are significantly lower than the mean values of igneous magnetite; the Ni contents analyzed by EMPA are even below the detection limit. In addition, magnetite from Dongping shows features of low Ti contents. Most of the current genetic discrimination diagram of magnetite does not present the locations of the Dongping type deposit. As shown in the genetic discrimination diagram of V vs. Ti and Ti vs. Ni/Cr, the analyzed spots from Dongping are mainly located around the field of “hydrothermal” [34–36], indicating that the magnetite are formed in the hydrothermal stage. Compared with magnetite in porphyry, skarn, IOCG, and Kiruna (IOA) deposit, magnetite from the Dongping deposit shows characteristics of variable Ca, Al, and Mn contents, with wide ranges of Ti + V values (Figure 8).

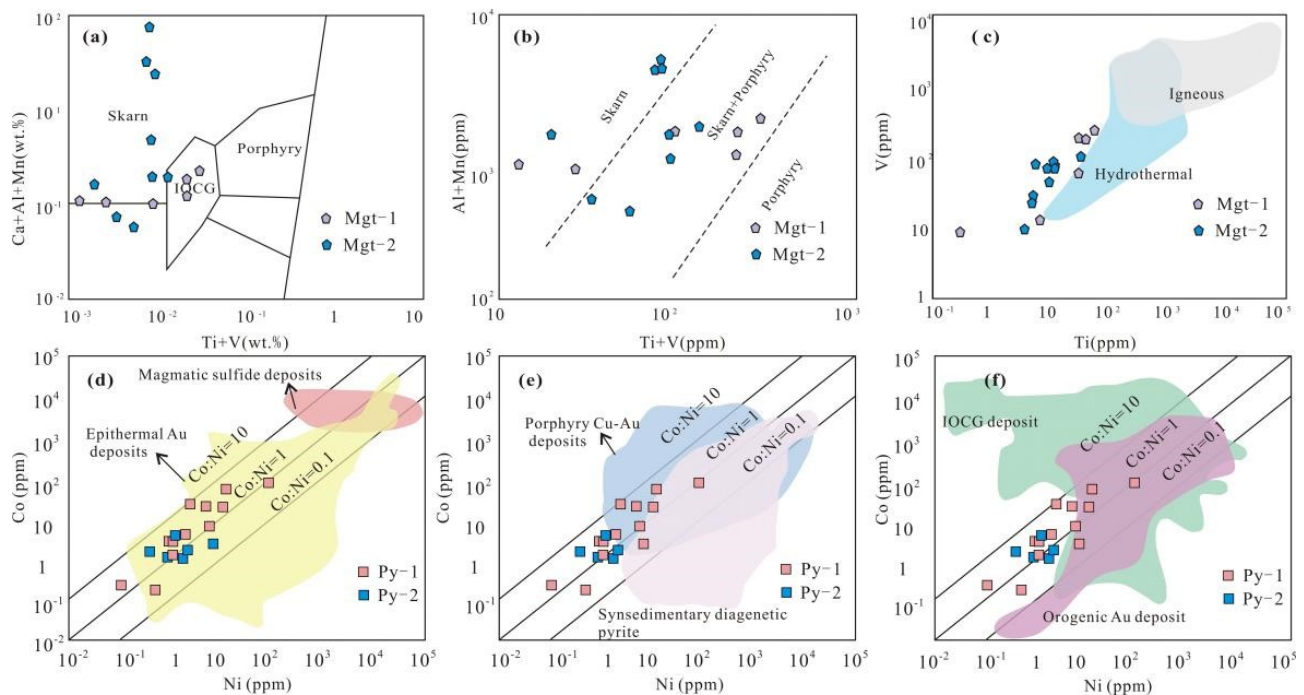


Figure 8. Genetic discrimination diagram for the magnetite and pyrite from Dongping deposit: (a) Ca + Al + Mn vs. Ti + V diagram for the magnetite; (b) Ni/(Cr + Mn) vs. Ti + V diagram for the magnetite [32]; (c) V vs. Ti for the magnetite [33,34]; (d–f) Co vs. Ni diagram for the pyrite [37]. The data used in the figure are from Tables 2 and 4.

6.2.2. Pyrite

Pyrite is the most common constituent of ore-bearing mineral assemblages in lode-type gold deposits [36,38]. As pyrites formed in different environments have distinctive compositional features, the minor and trace element contents can provide helpful information in determining the ore-forming processes. Co/Ni values of pyrite is the most sensitive indicators of the ore-forming environment. Generally, the higher Co/Ni mass ratio of pyrite ($\text{Co/Ni} > 1$) is attributed to magmatic hydrothermal origin, while pyrite with low Co/Ni ratio ($\text{Co/Ni} < 1$) is thought to be influenced by sedimentary materials [39,40].

Pyrite from the Dongping deposit has higher Co contents, but relatively lower Ni contents. The corresponding pyrite Co/Ni ratios from our EMPA analysis are significantly greater than 1.0. The LA-ICP-MS analytical results indicated that pyrites from Dongping have variable Co/Ni mass ratios ranging between 0.3 and 9.2 (Table 4), with an average of 2.3. In the Ni vs. Co plot, all of the samples from our analysis are located in the field of epithermal gold deposit, around the field of porphyry and orogenic gold deposits, which is also significantly different from magmatic sulfide deposits and IOCG deposits. Therefore, we propose that the ore-forming fluids of Dongping dominantly originate from a magmatic source, and incorporate some sedimentary materials from wall rock during the fluid migration.

6.3. Constraints on Hydrothermal Fluid Evolution

Even though the genetic type and formation age of Dongping deposit are still controversial, numerous C-H-O-S-Pb isotopic studies have also indicated that the ore-forming fluids of Dongping were dominantly magmatic hydrothermal in origin [41–43]. A remarkable feature of Dongping type mineralization is the presence of garnet in the ores, and the recent garnet U-Pb dating proved that the Dongping deposit formed at the age of 139–142 Ma, which is broadly coeval with the Early Cretaceous granitoid magmatism [44]. Our combined EMPA and LA-ICP-MS analysis on magnetite and pyrite further confirmed that the petrogenesis and metallogenesis in the Dongping district have a close temporal relationship, and the gold mineralization in this area are products of the Mesozoic tectonic-magmatic event.

In this study, two types of magnetite and two types of pyrite have been identified, providing us an excellent opportunity to trace the whole evolutionary process of ore-forming fluids. Element availability is the first-order control for minor and trace element contents in hydrothermal fluids. Spinel elements, such as Mn, Fe, Cu, Zn, As, Mo, Ag, Au, and Pb are commonly enriched in hydrothermal fluids compared to their content in igneous host rocks. Mn and Zn are widely incorporated into hydrothermal magnetite at levels above 100 ppm. In the Dongping deposit, Mn and Zn content in magnetite range 297–4348 ppm and 66.9–1707 ppm, respectively, which are significantly higher than the mean values of igneous magnetite. Contents of Cu, Au, Ag, and Mo in magnetite from Dongping are also similar to those of magmatic-hydrothermal deposits. Al and Ti are considered to be immobile during the fluid-rock reaction, and the incorporation of Al and Ti in magnetite is largely temperature-controlled. Therefore, the magnetite formed at hotter temperatures generally have higher Al and Ti contents, and the igneous magnetite has considerably higher Al and Ti contents than hydrothermal magnetite. Magnetite of this study have similar Al contents with porphyry deposit, but relatively lower Ti contents (average at 13.9 ppm), indicating that the magnetite from Dongping may be formed at a lower temperature condition than previously estimated. Considering also the fact that magnetite coexists with hematite, we can speculate that the magnetite in Dongping may have formed from relatively oxidizing fluids with lower temperatures.

The Co solubility in hydrothermal solutions is significantly influenced by temperature [45]. At Dongping, the Co contents from Py-1 to Py-2 shows a decreasing trend, indicating that the fluid temperature decreases continuously from the early to late stage. Compared with Py-1, the Cu, Zn, Ag, W, Au, Pb, and Bi, contents of Py-2 are relatively higher. The emission of CO₂ caused by the boiling of ore-forming fluids is considered to be an important mechanism for the precipitation of ore-forming materials in gold deposits. This is supported by a previous fluid inclusions study, which revealed that, the fluid heterogenization have occurred in the Dongping mineralization system [41].

7. Conclusions

1. Two magnetite sub-types, including disseminated magnetite in altered potassic igneous rocks and magnetite in quartz vein, and two pyrite sub-types, including pyrite

- in oxide-ore stage (Py-1), pyrite in gold-bearing sulfide-telluride-ore stage (Py-2), are identified in the Dongping deposit.
2. A combined EMPA and LA-ICP-MS analysis on magnetite reveals that magnetite from Dongping have lower Ti and V contents, as well as wide ranges of Al, Mn, and Ca contents, indicating that they are originated from magmatic-hydrothermal fluids rather than igneous origins. These magnetites are interpreted to have resulted from low-temperature conditions of hydrothermal activity.
 3. The average Au contents of pyrites from Dongping are relatively lower. The time-resolved signals of LA-ICP-MS of pyrite indicates that Co and Ni enter pyrite lattice by forming solid solutions, whereas Pb, Zn, and Cu mainly present as sulfide inclusions. From Py-1 to Py-2, Co shows a decreasing trend, indicating that the temperature of ore forming fluids has decreased. Combined with previous research of fluid inclusion, we infer that the enrichment of metal elements in Py-2 is related to the cooling or boiling of the fluids.

Author Contributions: Conceptualization, C.W. and Y.R.; methodology, Z.S.; software, C.W.; investigation, C.W.; J.Y.; J.Z.; data curation, J.Y.; writing—original draft preparation, C.W.; writing—review and editing, C.W. All authors have read and agreed to the published version of the manuscript.

Funding: This research was funded by the Youth fund of National Natural Science Foundation of China (Grant Number 42002093) and the Fundamental Research Funds for the Central Universities of China (Grant Number ZY20215134).

Acknowledgments: We sincerely appreciate the detailed and constructive reviews and suggestions from two anonymous reviewers, which greatly improved this paper. We especially thank Wuhan Sample Solution Analytical Technology Co., Ltd. for helping with the LA-ICP-MS trace element analyses.

Conflicts of Interest: The authors declare no conflict of interest.

References

1. Zhou, T.; Lü, G. Tectonics, granitoids and Mesozoic gold deposits in east Shandong, China. *Ore Geol. Rev.* **2000**, *16*, 71–90. [[CrossRef](#)]
2. Zhou, T.; Goldfarb, R.J.; Phillips, G.N. Tectonic and distribution of gold deposits in China—An overview. *Miner. Depos.* **2002**, *37*, 249–282. [[CrossRef](#)]
3. Yang, J.H.; Wu, F.Y.; Wilde, S.A. A review of the geodynamic setting of large-scale late mesozoic gold mineralization in the north china craton: An association with lithospheric thinning. *Ore Geol. Rev.* **2003**, *23*, 125–152. [[CrossRef](#)]
4. Zhai, M.G.; Santosh, M. The early Precambrian odyssey of the North China Craton: A synoptic overview. *Gondwana Res.* **2011**, *20*, 6–25. [[CrossRef](#)]
5. Zhao, G.C.; Sun, M.; Wilde, S.A.; Li, S.Z. Late Archean to Paleoproterozoic evolution of the North China Craton: Key issues revisited. *Precambr. Res.* **2005**, *136*, 177–202. [[CrossRef](#)]
6. Mao, J.W.; Li, Y.Q.; Goldfarb, R.J.; He, Y.; Zaw, K. Fluid inclusion and noble gas studies of the Dongping gold deposit, Hebei Province, China: A mantle connection for mineralization? *Econ. Geol.* **2003**, *98*, 517–534. [[CrossRef](#)]
7. Bao, Z.W.; Zhao, Z.H.; Zhang, P.H.; Wang, Y.X. Re, Sr, Nd, and Pb isotopic evidence for the petrogenesis of the Shuiquanguo syenite complex in nw hebei province. *Geol. Rev.* **2003**, *49*, 60–596.
8. Wang, D.; Liu, J.; Zhai, D.; Carranza, E.; Wang, Y.; Zhen, S.; Wang, J.; Wang, J.; Liu, Z.; Zhang, F. Mineral paragenesis and ore-forming processes of the dongping gold deposit, hebei province, China. *Resour. Geol.* **2019**, *69*, 287–313. [[CrossRef](#)]
9. Gao, S.; Xu, H.; Zhang, D.; Shao, H.; Quan, S. Ore petrography and chemistry of the tellurides from the dongping gold deposit, hebei province, China. *Ore Geol. Rev.* **2015**, *64*, 23–34. [[CrossRef](#)]
10. Bao, Z.; Sun, W.; Li, C.; Zhao, Z. U–Pb dating of hydrothermal zircon from the dongping gold deposit in north china: Constraints on the mineralization processes. *Ore Geol. Rev.* **2014**, *61*, 107–119. [[CrossRef](#)]
11. Bao, Z.W.; Li, C.J.; Zhao, Z.H. Metallogeny of the syenite-related Dongping gold deposit in the northern part of the North China Craton: A review and synthesis. *Ore Geol. Rev.* **2016**, *73*, 198–210. [[CrossRef](#)]
12. Zhao, G.C.; Cawood, P.A.; Li, S.Z.; Wilde, S.A.; Sun, M.; Zhang, J.; He, Y.H.; Yin, C.Q. Amalgamation of the North China Craton: Key issues and discussion. *Precambr. Res.* **2012**, *222–223*, 55–76. [[CrossRef](#)]
13. Deng, J.; Wang, Q.F. Gold mineralization in China: Metallogenic provinces, deposit types and tectonic framework. *Gondwana Res.* **2016**, *36*, 219–274. [[CrossRef](#)]
14. He, C.S.; Santosh, M.; Yang, Q.Y. Gold metallogeny associated with craton destruction: A geophysical perspective from the North China Craton. *Ore Geol. Rev.* **2016**, *75*, 29–41. [[CrossRef](#)]

15. Li, S.R.; Santosh, M. Geodynamics of heterogeneous gold mineralization in the North China Craton and its relationship to lithospheric destruction. *Gondwana Res.* **2017**, *50*, 267–292. [[CrossRef](#)]
16. Nie, F.J. Type and distribution of gold deposits along the northern margin of the North China Craton, People's Republic of China. *Int. Geol. Rev.* **1997**, *39*, 151–180. [[CrossRef](#)]
17. Song, G.R.; Zhao, Z.H. *Geology of Dongping Alkaline Complex-Hosted Gold Deposit in Hebei Province*; Seismological Press: Beijing, China, 1996; pp. 4–109. (In Chinese with English Abstract)
18. Li, C.M.; Deng, J.F.; Su, S.G.; Li, H.M.; Liu, X.M. Two stage zircon U–Pb ages of the potash altered rock in the Dongping gold deposit, Hebei Province, and their geological implications. *Acta Geosci. Sin.* **2010**, *31*, 843–852. (In Chinese with English Abstract)
19. Zhang, Z.C.; Mao, J.W. Geology and geochemistry of the Dongping gold telluride deposit, Hebei Province, North China. *Internat. Geol. Rev.* **1995**, *37*, 1094–1108.
20. Cisse, M.; Lü, X.; Algeo, T.J.; Cao, X.; Li, H.; Wei, M.; Chen, M. Geochronology and geochemical characteristics of the Dongping ore-bearing granite, North China: Sources and implications for its tectonic setting. *Ore Geol. Rev.* **2017**, *89*, 1091–1106. [[CrossRef](#)]
21. Gao, S.; Xu, H.; Li, S.; Santosh, M.; Zhang, D.; Yang, L.; Quan, S. Hydrothermal alteration and ore-forming fluids associated with gold-tellurium mineralization in the Dongping gold deposit, China. *Ore Geol. Rev.* **2017**, *80*, 166–184. [[CrossRef](#)]
22. Hu, Z.C.; Zhang, W.; Liu, Y.S.; Gao, S.; Li, M.; Zong, K.Q.; Chen, H.H.; Hu, S.H. "Wave" Signal-Smoothing and Mercury-Removing Device for Laser Ablation Quadrupole and Multiple Collector ICPMS Analysis: Application to Lead Isotope Analysis. *Anal. Chem.* **2015**, *87*, 1152–1157. [[CrossRef](#)] [[PubMed](#)]
23. Liu, Y.S.; Hu, Z.C.; Gao, S.; Günther, D.; Xu, J.; Gao, C.G.; Chen, H.H. In situ analysis of major and trace elements of anhydrous minerals by LA-ICP-MS without applying an internal standard. *Chem. Geol.* **2008**, *257*, 34–43. [[CrossRef](#)]
24. Cook, N.J.; Ciobanu, C.L.; Mao, J.W. Textural control on gold distribution in Asfree pyrite from the Dongping, Huangtuliang and Hougou gold deposits, North China Craton (Hebei Province, China). *Chem. Geol.* **2009**, *264*, 101–121. [[CrossRef](#)]
25. Nadoll, P.; Angerer, T.; Mauk, J.L.; French, D.; Walshe, J. The chemistry of hydrothermal magnetite: A review. *Ore Geol. Rev.* **2014**, *61*, 1–32. [[CrossRef](#)]
26. Ciobanu, C.L.; Cook, N.J.; Utsunomiyas, S.; Kogagwa, M.; Green, L.; Gilbert, S.; Wade, B. Gold–telluride nanoparticles revealed in arsenic-free pyrite. *Am. Miner.* **2012**, *97*, 1515–1518. [[CrossRef](#)]
27. Thomas, H.V.; Large, R.R.; Bull, S.W.; Malennikov, V.; Berry, R.F.; Fraaser, R.; Froud, S.; Moye, R. Pyrite and pyrrhotite textures and composition in sediments, laminated quartz veins, and reefs at Bendigo gold mine, Australia: Insights for ore genesis. *Econ. Geol.* **2011**, *106*, 1–31. [[CrossRef](#)]
28. Dare, S.A.S.; Barnes, S.J.; Beaudoin, G. Variation in trace element content of magnetite crystallized from a fractionating sulfide liquid, Sudbury, Canada: Implications for provenance discrimination. *Geochim. Cosmochim. Acta* **2012**, *88*, 27–50. [[CrossRef](#)]
29. Xie, Q.H.; Zhang, Z.C.; Hou, T.; Jin, Z.L.; Santosh, M. Geochemistry and oxygen isotope composition of magnetite from the Zhangmatun deposit, North China Craton: Implications for the magmatic-hydrothermal evolution of Cornwall-type iron mineralization. *Ore Geol. Rev.* **2017**, *88*, 57–70. [[CrossRef](#)]
30. Belousov, I.; Large, R.R.; Meffre, S.; Danyushevsky, L.V.; Steadman, J.; Beardsmore, T. Pyrite compositions from vhm and orogenic au deposits in the yilgarn craton, western australia: Implications for gold and copper exploration. *Ore Geol. Rev.* **2016**, *79*, 474–499. [[CrossRef](#)]
31. Craig, J.R.; Vokes, F.M.; Solberg, T.N. Pyrite: Physical and chemical textures. *Miner. Depos.* **1998**, *34*, 82–101. [[CrossRef](#)]
32. Dupuis, C.; Beaudoin, G. Discriminant diagrams for iron oxide trace element fingerprinting of mineral deposit types. *Miner. Depos.* **2011**, *46*, 319–335. [[CrossRef](#)]
33. Nadoll, P.; Mauk, J.L.; Leveille, R.A.; Koenig, A.E. Geochemistry of magnetite from porphyry Cu and skarn deposits in the southwestern United States. *Miner. Depos.* **2015**, *50*, 493–515. [[CrossRef](#)]
34. Dare, S.A.S.; Barnes, S.J.; Beaudoin, G.; Méric, J.; Boutroy, E.; Potvin-Doucet, C. Trace elements in magnetite as petrogenetic indicators. *Miner. Depos.* **2014**, *49*, 785–796. [[CrossRef](#)]
35. Hu, H.; Li, J.W.; Lentz, D.; Ren, Z.; Zhao, X.F.; Deng, X.D.; Hall, D. Dissolution reprecipitation process of magnetite from the Chengchao iron deposit: Insights into ore genesis and implication for in-situ chemical analysis of magnetite. *Ore Geol. Rev.* **2014**, *57*, 393–405. [[CrossRef](#)]
36. Goldfarb, R.J.; Baker, T.; Dubé, B.; Groves, D.I.; Hart, C.J.R.; Gosselin, P. Distribution, character, and genesis of gold deposits in metamorphic terranes. In *Economic Geology 100th Anniversary Volume*; Society of Economic Geologists: Littleton, CO, USA, 2005; pp. 407–450.
37. Wang, K.; Zhai, D.; Liu, J.; Wu, H. LA-ICP-MS trace element analysis of pyrite from the Dafang gold deposit, South China: Implications for ore genesis. *Ore Geol. Rev.* **2021**, *139*, 104507. [[CrossRef](#)]
38. Koglin, N.; Frimmel, H.E.; Minter, W.; Brätz, H. Trace-element characteristics of different pyrite types in mesoarchean to palaeoproterozoic placer deposits. *Miner. Depos.* **2010**, *45*, 259–280. [[CrossRef](#)]
39. Braliala, A.; Sabatini, G.; Troja, F. A reevaluation of the Co/Ni ratio in pyrite as geochemical tool in ore genesis problems. *Miner. Depos.* **1979**, *14*, 353–374. [[CrossRef](#)]
40. Clark, C.; Grguric, B.; Mumm, A.S. Genetic implications of pyrite chemistry from the Palaeoproterozoic Olary Domain and overlying Neoproterozoic Adelaidean sequences, northeastern South Australia. *Ore Geol. Rev.* **2004**, *25*, 237–257. [[CrossRef](#)]
41. Fan, H.; Xie, Y.; Zhai, M. Ore-forming fluids in the dongping gold deposit, northwestern hebei province. *Sci. China Ser. D Earth Sci.* **2001**, *44*, 748–757. [[CrossRef](#)]

42. Zhang, G.R.; Xu, J.H.; Wei, H.; Song, G.C.; Zhang, Y.B.; Zhao, J.K.; He, B.; Chen, D.L. Structure, alteration, and fluid inclusion study on the surrounding area of the Dongping gold deposit, northern Hebei, China. *Acta Petrol. Sin.* **2012**, *28*, 637–651. (In Chinese with English Abstract)
43. Nie, F.J. Geology and origin of the Dongping alkali-type gold deposit, Northern Hebei Province, People's Republic of China. *Resour. Geol.* **1998**, *48*, 139–158. [[CrossRef](#)]
44. Fan, G.H.; Li, J.W.; Deng, X.D.; Gao, W.S.; Li, S.Y. Age and origin of the Dongping Au-Te deposit in the North China Craton revisited: Evidence from paragenesis, geochemistry, and in situ U-Pb geochronology of garnet. *Econ. Geol.* **2021**, *116*, 963–985. [[CrossRef](#)]
45. Migdisov, A.A.; Zevin, D.; Williams-Jones, A.E. An experimental study of cobalt (ii) complexation in cl and h₂s-bearing hydrothermal solutions. *Geochim. Cosmochim. Acta* **2011**, *75*, 4065–4079. [[CrossRef](#)]